PFC/JA-90-8

Operation of a Long-Pulse Magnetron in a Phase-Locked System

Chen, S.C.; Bekefi, G.; Temkin, R.J.

Plasma Fusion Center
Massachusetts Institute of Technology
Cambridge, MA 02139

February 1990

This work was supported by Harry Diamond Labs (Army) Contract DAAL02-89-K-0084.

Operation of a Long-pulse Relativistic Magnetron in a Phase-locking system

Shien-Chi Chen, George Bekefi, and Richard Temkin

Plasma Fusion Center
Massachusetts Institute of Technology, Cambridge, MA 02139

ABSTRACT

Successful injection-locking of relativistic magnetrons requires frequency stable microwave output with pulse lengths longer than the phase-locking time. We report the major experimental results from our stable and long-pulse relativistic magnetron system designed to address important issues relevant to the realization of injection-locking. Long voltage pulse operation ($> 1\mu$s) with good stability was achieved, and relatively long (250 ns) RF pulses at 5 MW output power level were generated. These pulses exceed the theoretical locking time for a 1 MW injected power source. The magnetron operates in S-band (3.66 GHz) and is driven by a modulator which operates either at 700 kV/ 700 A or 250 kV/ 1.7 kA. The stability of the narrow band microwave frequency is better than 3 parts in 1000. Possible RF pulse-shortening mechanisms are studied.

1. INTRODUCTION

Phase-locking of relativistic magnetrons has been a subject of intensive experimental[1-3] and theoretical[4-6] research. The successful demonstration of phase stability and phase-locking of such oscillators could lead to the realization of multi-gigawatt RF power generation in the microwave regime, which would have important impact on a variety of fields such as defense applications, particle acceleration, communication, and power transmission.

Injection locking of relativistic magnetrons using a relatively low power reference signal requires the following conditions being satisfied: (1) the free-running frequency must be close enough to the injection frequency, and remain within the Adler locking bandwidth throughout the pulse duration; (2) the relativistic magnetron oscillation must last longer than the required phase-locking time. Relativistic magnetrons, like all high power oscillators, are short-pulsed in nature, typically less than 50 ns. The phase-locking time for these low Q oscillators, however, is on the order of a few hundred RF-cycles (depending on the injection power level).[6] To achieve phase-locking, it is necessary to understand

issues concerning the power stability, spectral purity, and the phase characteristics of relativistic magnetrons under long pulse operation. Experimentally, it has been extremely difficult to produce long-pulse microwave output at high powers from Marx-based relativistic magnetrons.[7-9]

This paper describes the experimental results of a long-pulse relativistic magnetron system driven by a stable high voltage modulator. The major operating characteristics, relevant to phase-locking, are discussed. Section 2 describes the experimental setup. In section 3, experimental results are discussed. Subsections in section 3 deal with important operating features, including: the dynamic impedance of cold-cathode relativistic magnetrons; the output power and efficiency; the voltage pulse length and stability; the RF pulse length; and the mode and frequency stability. Section 4 summarizes and discusses the main results.

2. APPARATUS

The experimental setup is shown schematically in Fig. 1. The transformer-based high power modulator produces 700 kV, 780 A , 2 μs pulses with a repetition rate of 4 Hz. The high voltage pulses are delivered through the cathode shank to the magnetron cathode. The anode is held at ground potential to maintain the voltage drop across the anode-cathode gap. The relativistic magnetron diode is located at the center of the bore of a superconducting magnet capable of generating uniform DC fields up to 22 kG. The vacuum system is evacuated through a pumping port. The electron current is monitored at two places: the total current is measured with a current viewing resistor (CVR) embedded in the return path; the axial current is collected downstream and measured with another CVR. Microwave output is extracted radially in waveguide through the radial access holes in the superconducting magnet. The injection signal for the phase locking experiment is launched through another radial access hole into the magnetron interaction region. The injection RF source is a 1 MW, 1 μs conventional magnetron, with frequency tunable from 3.1 GHz to 3.5 GHz. The detail of the experimental setup can be found in previous papers.[2,3]

3. EXPERIMENTAL RESULTS

3.1 Relativistic magnetron impedance

The magnetron impedance Z of a cold-cathode field-emission system is a dynamical quantity which plays an important role in achieving high power operation. The relativistic

magnetron impedance Z is determined by the interplay between the nonlinear field emission process under the applied anode voltage V and the magnetic insulation process under the applied transverse magnetic field B

$$Z = Z(g,\ V,\ B,\ ...) \tag{1}$$

where g is the anode-cathode gap. It should be noted that the anode voltage, in turn, depends on the magnetron impedance

$$V = V_{matched} \cdot \frac{2\frac{Z}{Z_{p.s.}}}{(1+\frac{Z}{Z_{p.s.}})} \tag{2}$$

where $V_{matched}$ is the anode voltage under matched condition and $Z_{p.s.}$ is the power supply impedance. The nonlinear interdependence between Z and V (Eqs. (1) and (2)) is an interesting phenomenon deserving further experimental and theoretical study. Under operating conditions, the presence of the strong electromagnetic field, whose electric field component is comparable to the applied DC field, further complicates things. In general, the dependence of the cold-cathode relativistic magnetron impedance on the operating parameters is very complicated and cannot be calculated from first principles.

To characterize the impedance behavior empirically, we compiled data obtained in previous experiments and generated a plot of magnetron impedance as a function of the physical A-K gap at various diode voltages (see Fig. 2). The magnetic fields used in obtaining these data points are related to the operating voltages through the Buneman-Hartree condition. The data points lie on curves that indicate the following trend: larger A-K gaps lead to higher impedances; higher applied voltages draw more current from the cathode and hence result in lower impedances. The seemingly simple empirical chart (Fig. 2) conveniently serves the purpose of predicting impedance characteristics of cold-cathode relativistic magnetrons. However, the underlying physics remains to be modeled.

The operating impedance determines the efficiency of power transfer from the power supply to the relativistic magnetron. The power transferred to the magnetron P_{in} is a fraction of the maximum power available under matched condition $P_{matched}$

$$P_{in} = P_{matched} \cdot \frac{4\frac{Z}{Z_{p.s.}}}{(1+\frac{Z}{Z_{p.s.}})^2}. \tag{3}$$

However, only a fraction of P_{in} is available for generating microwaves. In relativistic magnetrons, it is observed experimentally that an appreciable part of the current is lost

in the axial direction and does not participate in the interaction. The ratio of the radial (anode) current I_r to the total current I is a function of the aspect ratio g/l, where g is the A-K gap, and l is the anode length. Under resonance conditions, we observed a current ratio of 1/3 (see Fig. 3) for one of our magnetrons. The efficiency of the relativistic magnetron interaction η depends on the size of the A-K gap and the voltage applied across it, and is typically between 10% and 25%. Therefore, the output RF power is related to the power delivered from the power supply by

$$P_{RF} = P_{in}(\frac{Z}{Z_{p.s.}}) \cdot \frac{I_r}{I}(\frac{g}{\ell}) \cdot \eta(g,\ V, ...). \tag{4}$$

The output power thus depends on many interdependent parameters

$$P_{RF} = P_{RF}(Z,\ V,\ g, ...), \tag{5}$$

the proper choice of parameter combinations is therefore important in realizing highly efficient microwave generation systems.

3.2 Output power and efficiency

A prerequisite for efficient microwave generation is the effective power transfer from the power supply to the operating tube, that is, there must be a good matching between the impedances of the modulator and the relativistic magnetron. In the experiment, in order to better match the impedances, both the high power modulator and the magnetron designs were greatly modified. First, the impedance of the modulator was reduced from 900Ω to 144Ω by changing from a 20:1 to an 8:1 pulse transformer. Then, the experiment was carried out using a large gap (1.35 cm) magnetron structure, designated SM-1, running at lower voltages.

The design of the magnetron structure is of equal importance with the impedance matching consideration. One needs a good diode design to maximize growth rate of the designed operating mode. The A6 magnetron has been demonstrated to produce high powers with high efficiency; however, its small A-K gap leads to an impedance too low for our modulator (see Fig. 2). Instead, the SM-1 magnetron was fabricated and tested in the experiment. The radii of the cathode, the anode, and the vanes are 0.57 cm, 1.92 cm, and 3.42 cm, respectively. The full angle of the resonator opening is 20°. The large-gap magnetron SM-1 provides a better impedance match and facilitates long voltage pulses which are crucial in injection locking. It should be noted that a large gap, according to

Eqs. (1)-(5) and Fig. 2, reduces the diode voltage and increases the axial current loss, which results in low output power. In essence, long pulse operation is achieved at the expense of microwave peak power in our experiment. The low efficiency ($\approx 1\%$) was confirmed in our experiment as well as in 2D MAGIC simulation.[10]

Typical waveforms for voltage and currents (both axial and total) are shown in Fig. 4. The voltage pulse remains flat for 1 μs (bottom trace), and varies less than $\pm 0.5\%$ in the first 500 ns. The axial current (top trace) is collected downstream and measured by a Faraday cup. The axial-current waveform follows that of the voltage. The middle trace of Fig. 4 shows the evolution of the total current, which increases monotonically until the voltage drops to zero. Fig. 5 shows the Hull cutoff and the resonance curves for the π and the 2π modes. The operating points (circles) and the corresponding microwave output (triangles) for the SM-1 anode with a retracted velvet washer cathode are shown in the Figure. The effects of the nonlinear dynamic impedance of the relativistic magnetron, as described in 3.1, are visible in Fig. 5. By fixing the charging voltage and scanning the magnetic field, the diode becomes more insulated with higher magnetic filed, and the impedance increases accordingly. The upward trend of the operating voltage continues until it is limited by the power supply. The operating points lie between the two resonance curves, and the strongest microwave output is observed when the operating point is close to the π-mode resonance condition. The maximum microwave peak power measured so far is 5 MW.

Measurements were also made on the power extracted from the axial direction, with 300 W observed in S-band and 10 W in C-band. The axial power level is typically 40 dB lower than the radial output.

3.3 Voltage pulse length and stability

Contrary to experience with short-pulse relativistic magnetrons, it was found that a vacuum of better than 1 x 10^{-6} is essential for sustaining the whole voltage pulse. This fact was demonstrated in the following experiments. In a planar diode experiment using 8 cm diameter electrodes (4.2 cm emitter diameter) with a 3 cm gap, the diode showed a strong dependence on the operating vacuum. When the pressure in the gap region was 4 x 10^{-4} Torr, the diode broke down before reaching the maximum voltage, which resulted in voltage pulse lengths of 300 ns. With the vacuum improved by two orders of magnitude to 4 x 10^{-6} Torr, the diode voltage reached a value agreeing with the Child-Langmir law, and lasted for more than 2 μs. The importance of vacuum was also seen in a

separate experiment running with a smooth bore magnetron with an overlong cathode. Six successive shots were fired at 1 second intervals. During the firing sequence, the 9 x 10^{-5} Torr base vacuum was increased to 5 x 10^{-4} Torr and the voltage pulse length was reduced on a shot-to-shot basis from 1.5 μs to 0.5 μs.

The relativistic magnetron vacuum system has since been improved: plastic parts (except for the voltage insulator) have been replaced by quartz; all bakable sections have been baked out; grease content has been kept to a minimum (except for the voltage insulator). A base pressure of 8 x 10^{-7} Torr is achieved.

Cathode materials determine the microscopic nature of the field-emission , and hence the available voltage pulse lengths. It has been reported in our previous experiment that velvet-lined cathodes produce longer voltage and microwave pulses.[2] In the present experiment the SM-1 diode has demonstrated 2 μs voltage pulses with 250ns microwave output using a velvet cathode. In sharp contrast, the graphite cathode produces a 350 ns voltage pulse with a 100ns RF output.

Another technique of producing flat and stable long voltage pulses in running relativistic magnetrons is described as follows. During the relativistic magnetron interaction, due to the expanding cathode plasma, the effective A-K gap reduces as a function of time. Thus more and more current is drawn and the impedance is monotonically reduced during the pulse. This fact manifests itself through a slight voltage droop and a current increase in our scope traces (Fig. 4). To maintain the Buneman-Hartree condition, it is important that the voltage pulse is held flat. The pulse forming network (PFN) in our modulator is tunable by varying the inductances in the individual sections. We have demonstrated the capability to tune the PFN so that under matched conditions it produces a rising slope large enough to pre-compensate for the voltage droop under running condition.

The achievable pulse length of the voltage flat top is reduced at voltages higher than 200 kV (see Fig. 6). Also plotted in Fig. 6 is the corresponding microwave output pulse length under resonance condition, which is consistently shorter than the voltage pulse. The RF pulse-shortening phenomenon will be described next.

3.4 RF pulse length

The shortening of RF pulse relative to the applied voltage pulse has been observed in high power microwave (HPM) devices such as MILO, VIRCATOR, RK, RG, and BWO.

Speculations abound about possible mechanisms behind the pulse-shortening phenomenon. Our experiment runs at 5 MW level with a stable $1\mu s$ long voltage flat top and provides a unique window for studying this phenomenon in relativistic magnetrons. As Fig. 6 indicates, the microwave pulses are significantly shorter than the corresponding voltage pulses. Some of the possible causes are discussed in the following paragraphs: plasma motion closing the A–K gap; voltage fluctuation driving the interaction out of resonance; RF breakdown at the vane tips or the output port(s); and ion species present in the gap region interfering with the magnetron interaction.

In our experiment, the voltage pulses remain flat to within $\pm$ 2% for more than 500ns in some cases (Fig. 4). The corresponding RF pulse lengths are on the order of 200ns. Our large gap experiment shows that the voltage pulse remains flat and the impedance does not collapse within the first 500 ns, thus reducing the importance of the role gap closure play in long pulse relativistic magnetrons. The above observation also precludes the second mechanism — the voltage fluctuation quenching the interaction — as the sole mechanism responsible for the pulse-shortening.

RF breakdown was not seen in our experiment since the output power involved (5 MW) was relatively low compared to those in the other HPM experiments. Visual inspection of the output window and the anode structure after intensive running of the system showed no significant breakdown damage. The absence of RF breakdown was also reinforced by the direct photographic imaging of the interaction region.

By mounting a camera directly downstream and viewing along the axial direction, we obtained time integrated photographs of the interaction region of an operating magnetron (Fig. 7). The visible glow near the electrodes is believed to be from ions in the plasmas and the visible patterns may not be related to the electron–spoke dynamics at all. Main features observed include:

- Reproducible hot spots (strongest emission points) on the cathode surface are visible around the cathode, on top of the otherwise uniform glow. No feature extends radially outward from the emission surface (Fig. 7).
- Alternate vane tips of the anode segments are lit due to the electron spoke bombardment and the subsequent plasma formation. The locations of the bombarded vane tips are consistent with the sense of rotation of the electron spokes. The brightness increases with increasing diode voltage, current, and voltage duration (Figs. 7(a)–(c)).
- The anode plasma from the vane tips form visible flares. The trajectories of the "jets" indicate motion in both the radial and azimuthal direction (Figs. 7(b) and 7(c)). The

sense of the apparent "azimuthal rotation" is contrary to that of the electron spokes and is believed to be due to motion of positive ions.

The time integrated visual information thus obtained indicates that there is more plasma motion of the anode plasma than the cathode plasma (Figs. 7(b) and 7(c)). All trajectories of the luminosity have smooth curvatures, and no cross-gap arcing pattern is present. The diagnostics further reinforce the statement that neither gap closure nor RF breakdown is solely responsible for the pulse-shortening. It is believed that out of the possible mechanisms listed above, the presence of ion species in the interaction region seems to be the most likely cause of pulse-shortening in our experiment. The plasmas may interfere with the electron dynamics and quench the gain process through the development of instabilities. It may happen to such an extent that the quenched magnetron interaction is beyond restart on the 1 μs time scale, as was experimentally observed. It is interesting to note that in conventional magnetrons, the interaction sustains for more than 1 μs at MW level routinely without troubles. By running our experiment at low voltage (60 kV) with low output power (20 kW), the full 1μs microwave pulse was recovered.

The RF output waveform, independent of its operating power level, was always spiky. This may be a direct result of the spiking characteristics of the field emission process at the cathode in cold-cathode relativistic magnetrons.

3.5 Mode and frequency stability

It was observed in previous experiments that the excitation of $\frac{2}{3}\pi$ mode besides the usual 2π mode is possible through voltage variation and through magnetic field tuning.[2] To achieve phase locking, the frequency fluctuation (shot-to-shot or variation within single pulse) has to be held within the narrow locking bandwidth. To obtain stable single-mode operation in relativistic magnetrons, it is imperative to use flat voltage pulses and use a diode design with good mode separation. As is seen in Fig. 5 the resonance line for the π–mode of the SM-1 magnetron no longer coincides with that of the 2π–mode to discourage mode competition. The cold test mode spectrum agrees with the frequencies of the 2D calculation (corrected for axial modes) to within 1%.

The operating frequency was measured using a surface-acoustic-wave device (SAW). The center frequency was measured to be 3660 MHz with a L.O. frequency of 2700 MHz (see Fig. 8). The apparent full width at half power point is about 12 MHz. This is to be compared with the typical pulse lengths of 100–250 ns (10—4 MHz). The frequency

stability was carefully characterized: the measured total shot-to-shot variation of center frequency was less than 15 MHz, part of which was due to the 200 ns firing time jitter (5 MHz). To achieve high stability, the applied magnetic field and diode voltage have to be stable on the 1 μs time scale; a space uniform and steady-state magnetic field was provided by a superconducting magnet specially designed for the experiment; a voltage flat top of less than $\pm 2\%$ variation was supplied by our high power modulator.

The frequency stability achieved in the experiment was suitable for subsequent phase-locking experiment. It is also interesting to note that voltage (and magnetic field) tuning of the relativistic magnetron was observed in our experiment. With a $\pm 10\%$ change in voltage, the corresponding frequency shift was about ± 20 MHz. We attribute most of the frequency shift to the frequency pushing, i.e. the dependence of operating frequency on the anode current. The frequency pushing effect, in theory, may play an important role in the phase-locking of relativistic magnetrons.[6]

4. DISCUSSION

Stable long voltage pulse ($> 1\mu s$) operation of a relativistic magnetron system was achieved using velvet-lined field-emission cathodes. Microwave output, 250 ns in length, at 5 MW (unoptimized) were obtained in the experiment with an efficiency of 5%. Axial current was found to be comparable with the radial current and will have to be suppressed to further increase the efficiency. Visual diagnostics and the voltage pulse shape indicated no shorting of the A–K gap in 1 μs. No evidence of RF breakdown was observed at this power level. The presence of high density ions in the interaction region was identified as the main cause of RF pulse–shortening in our experiment.

The large gap magnetron design (SM–1) leads to the expected π–mode operation. The measured operating frequency agrees well with the calculated and the cold–test values, the shot-to-shot frequency stability was better than 15 MHz, which is within the phase-locking bandwidth for our parameters. The measured bandwidth (12 MHz) is comparable with the instrument width. The 250 ns output pulse length is longer than the locking time required for phase-locking using 1 MW injection power source.

5. ACKNOWLEDGEMENT

This work was supported by Strategic Defense Initiative Organization, Office of Innovative Science and Technology, and managed by Harry Diamond Laboratories.

REFERENCE

1. J. Benford, H.M. Sze, W. Woo, R.R. Smith, and B. Harteneck, "Phase locking of relativistic magnetrons," *Phys. Rev Lett.*, vol. 62, pp. 969-971, 1989.

2. S.C. Chen and G. Bekefi, "Relativistic magnetron research," N. Rostoker, Editor, *Proc. SPIE*, vol. 873, pp 18-22, 1988.

3. S.C. Chen, G. Bekefi, R. Temkin, and C. de Graff, "Proposed injection locking of a long pulse relativistic magnetron," H.E. Brandt, Editor, *Proc. SPIE*, vol. 1061, pp. 157-160, 1989.

4. W. Woo, J. Benford, D., Fittinghoff, B. Harteneck, D. Price, R. Smith, and H. Sze, "Phase locking of high-power microwave oscillators," *J. Appl. Phys.*, vol. 65, pp. 861-866, 1989.

5. J.E. Walsh, G.L. Johnston, R.C. Davidson, and D.J. Sullivan, "Theory of phase-locked regenerative oscillators with nonlinear frequency-shift effects," *SPIE Proceedings*, vol. 1061, pp. 161-169, 1989.

6. S.C. Chen "Growth and frequency pushing effects in relativistic magnetron phase-locking", in this volume.

7. A.G. Nokonov, I.M. Roife, Yu.M. Savel'ev, and V.I. Éngel'ko, "Production of intense microsecond electron beams in a magnetron diode," *Sov. Tech. Phys.*, vol. 32, pp. 50-54, 1987.

8. A.N. Didenko, A.S. Sulakshin, G.P. Fomenko, V.I. Tsvetkov, Yu. G. Shtein, and Yu.G.Yushkov, "Relativistic magnetron with microsecond pulse lengths," *Sov. Tech. Phys. Lett.*, vol. 4, pp. 331-332, 1979.

9. I.Z. Gleizer, A.N. Didenko, A.S. Sulakshin, G.P. Fomenko, and V.I. Tsvetkov, "Limitation on the duration of the microwave emission in a high current magnetron," *Sov. Tech. Phys. Lett.*, vol. 6, pp. 19-20, 1980.

10. R.C. Davidson and C. Chen, private communication.

FIGURE CAPTIONS

Figure 1 The transformer-based modulator (1) produces high power pulses, which are delivered through the cathode shank (2) to the magnetron cathode (3). The anode (4) is held at ground potential to maintain the voltage drop across the anode-cathode gap. The relativistic magnetron diode is located in the center of the bore of a superconducting magnet (5). The vacuum system is evacuated through a pumping port (6). The electron current is monitored at two places: the total current is measure with a current viewing resistor (CVR) embedded in the return path (7); the axial current is collected downstream and measured with another CVR (8). Microwave output is extracted radially in waveguide through the radial access holes (9) in the superconducting magnet. The injection signal for the phase locking experiment is launched through another radial access hole (10) into the magnetron interaction region.

Figure 2 Diode impedance as a function of the A–K gap in cold-cathode relativistic magnetrons. The experimental points lie on various operating voltage curves. The A–K gap of A6 is 0.53 cm; the 0.83 gap diode is the A6 anode with a smaller diameter washer cathode; the 1.35cm gap is the SM-1 diode.

Figure 3 Current distribution of relativistic magnetron SM-1 under resonance condition as a function of operating voltage. The difference between the total and axial current is the radial current which is involved in the gain mechanism. The ratio of radial to total current is about 1/3.

Figure 4 Scope traces of axial current (top, 200 A/div), total current (middle, 500 A/div), and diode voltage (bottom). The time axis is 500 ns/div.

Figure 5 Operating characteristics of SM-1 magnetron with a charging voltage of 48kV. The three solid curves are the Hull cutoff, the π-mode and the 2π-mode resonance lines, respectively. The operating points (circles), namely the voltage as a function of magnetic field, demonstrate the effect of the interaction between the nonlinear relativistic magnetron impedance and the finite power supply impedance. Microwave output (triangles) peaks near the π-mode resonance. Maximum RF output is 5 MW.

Figure 6 Measured pulse lengths of the diode voltage and the output microwave as functions of the operating voltage.

Figure 7 Time integrated photograph of the magnetron interaction region. (a) Operating at 60 kV, the cathode is not completely turned on, the development of hot-spots on the cathode is clearly visible. (b) Operating at 150 kV with a voltage pulse length of

400 ns. (c) Operating at 150 kV with a voltage pulse length of 800 ns. Alternate vane tips of the anode segments are lit due to the electron spoke bombardment and the subsequent plasma formation. The locations of the bombarded vane tips are consistent with the sense of rotation of the electron spokes. The brightness increases with increasing diode voltage, current, and voltage duration The anode plasma from the vane tips form visible flares. The trajectories of the "jets" indicate motion in both the radial and azimuthal direction. The sense of the apparent "azimuthal rotation" is contrary to that of the electron spokes and is believed to be due to motion of positive ions. There is no evidence of cross-gap arcing.

Figure 8 Frequency spectrum (500 MHz/div) measured with a SAW device. The center frequency is 3660 GHz, with a 3 dB bandwidth of 12 MHz. Shot-to-shot frequency variation was less than 15 MHz, part of which was due to firing time jitter.

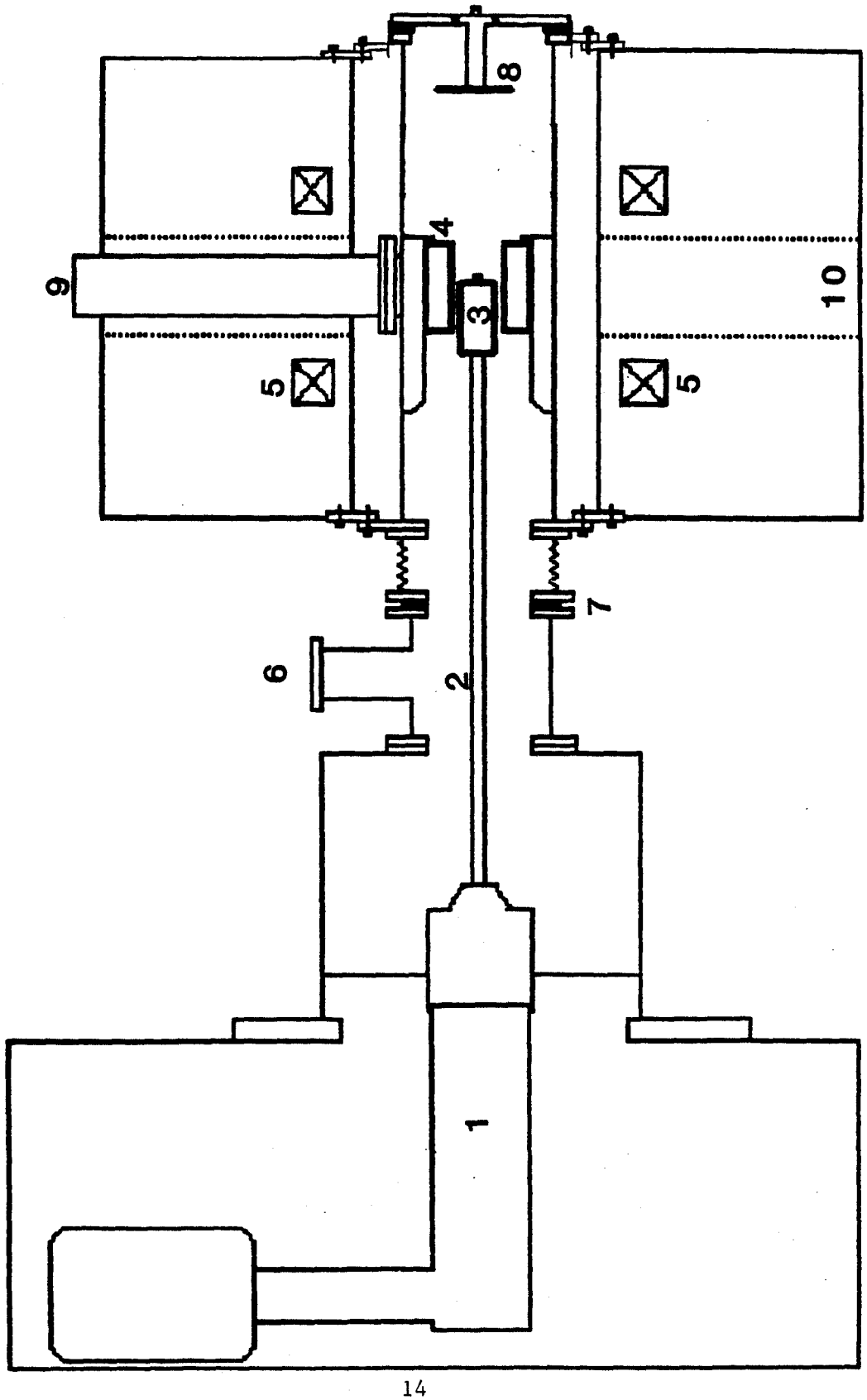

Fig. 1

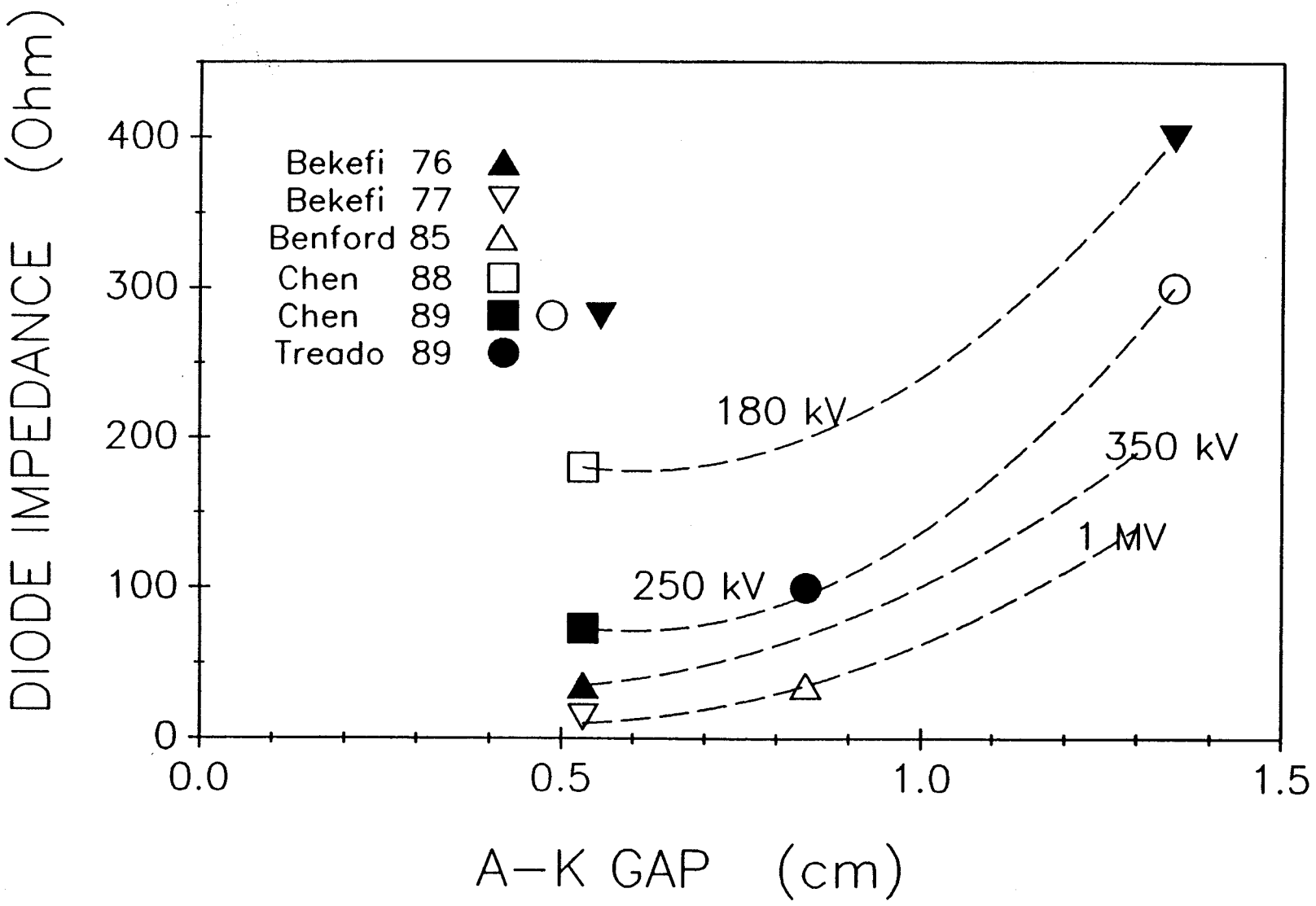
DIODE IMPEDANCE (Ohm)
400
300
200
100
0
0.0
0.5
1.0
1.5
A–K GAP (cm)
Bekefi 76
Bekefi 77
Benford 85
Chen 88
Chen 89
Treado 89
180 kV
250 kV
350 kV
1 MV

Fig. 2

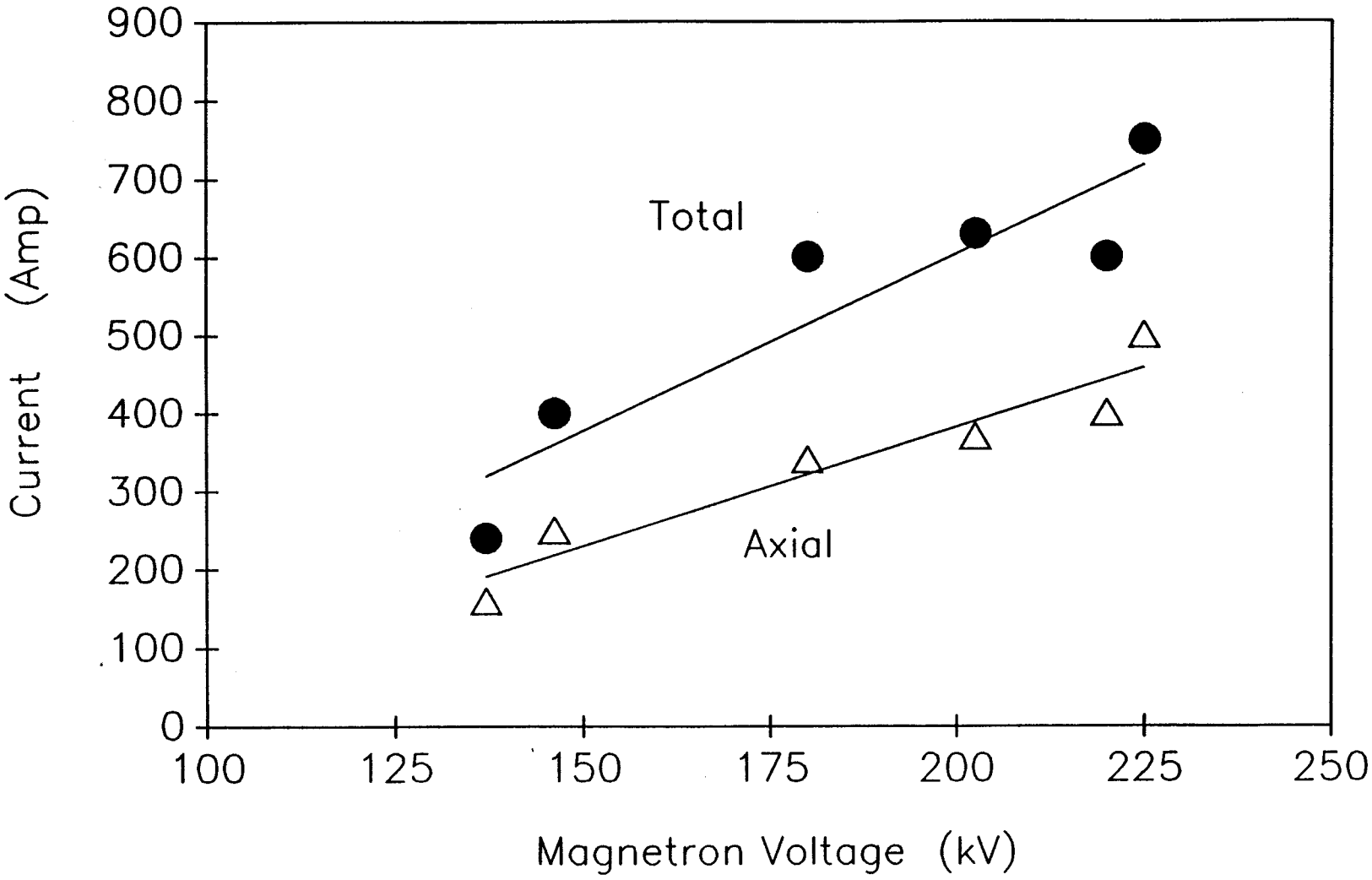
900
800
700
600
500
400
300
200
100
0
Current (Amp)
Total
Axial
100
125
150
175
200
225
250
Magnetron Voltage (kV)

Fig. 3

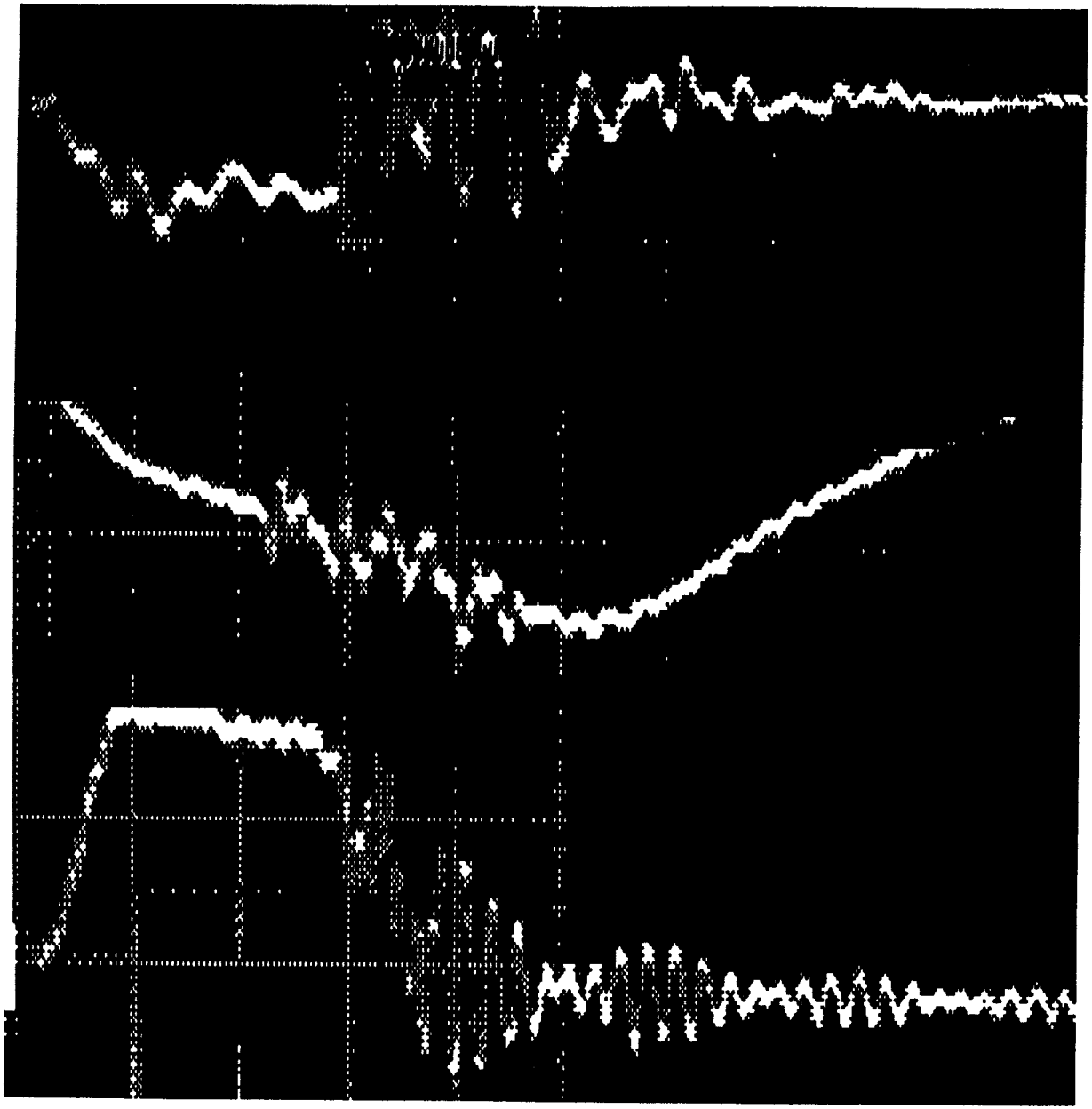

Fig. 4

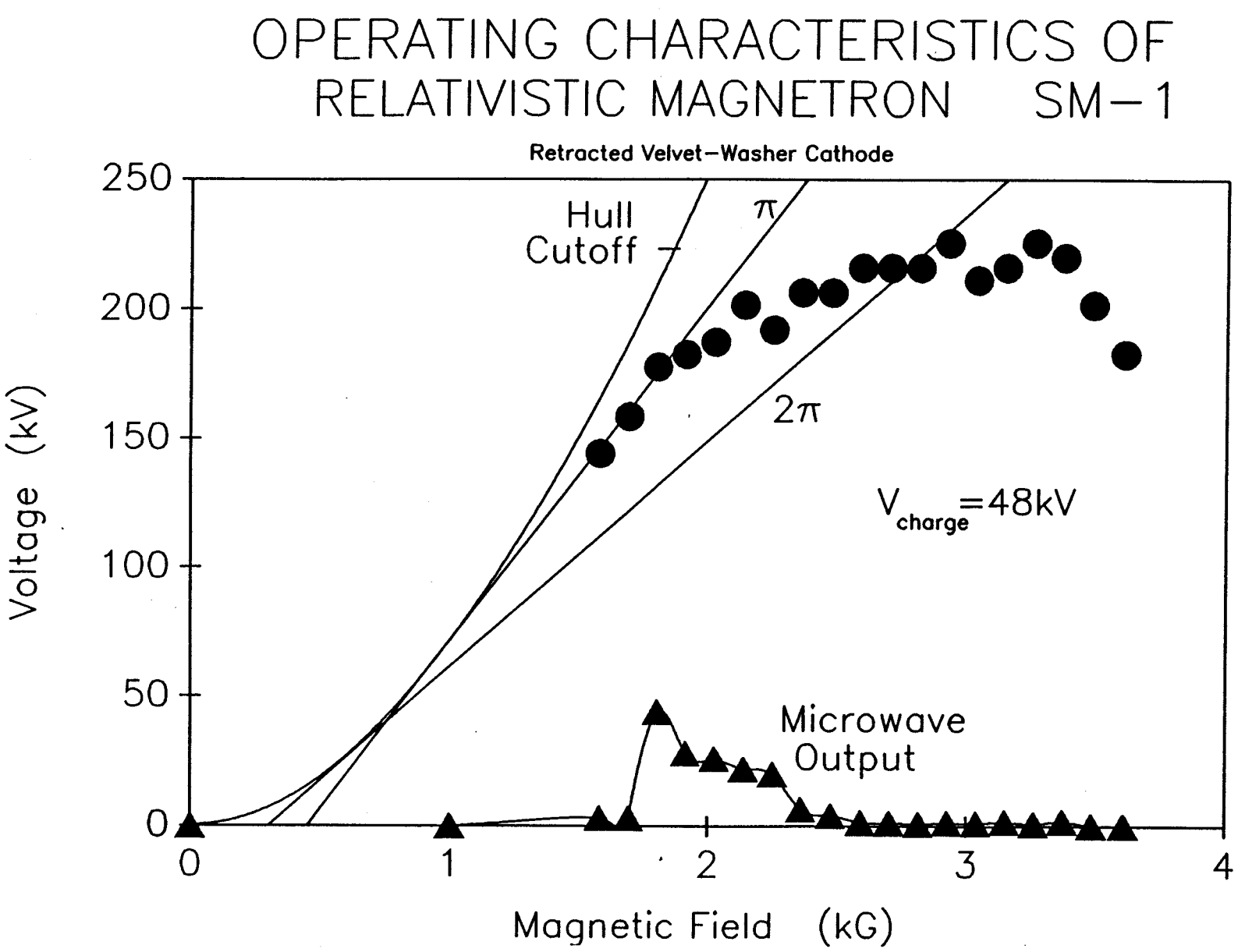
OPERATING CHARACTERISTICS OF
RELATIVISTIC MAGNETRON SM-1
Retracted Velvet-Washer Cathode
Hull
Cutoff
π
2π
V_{charge}=48kV
Microwave
Output
Voltage (kV)
250
200
150
100
50
0
0
1
2
3
4
Magnetic Field (kG)

Fig. 5

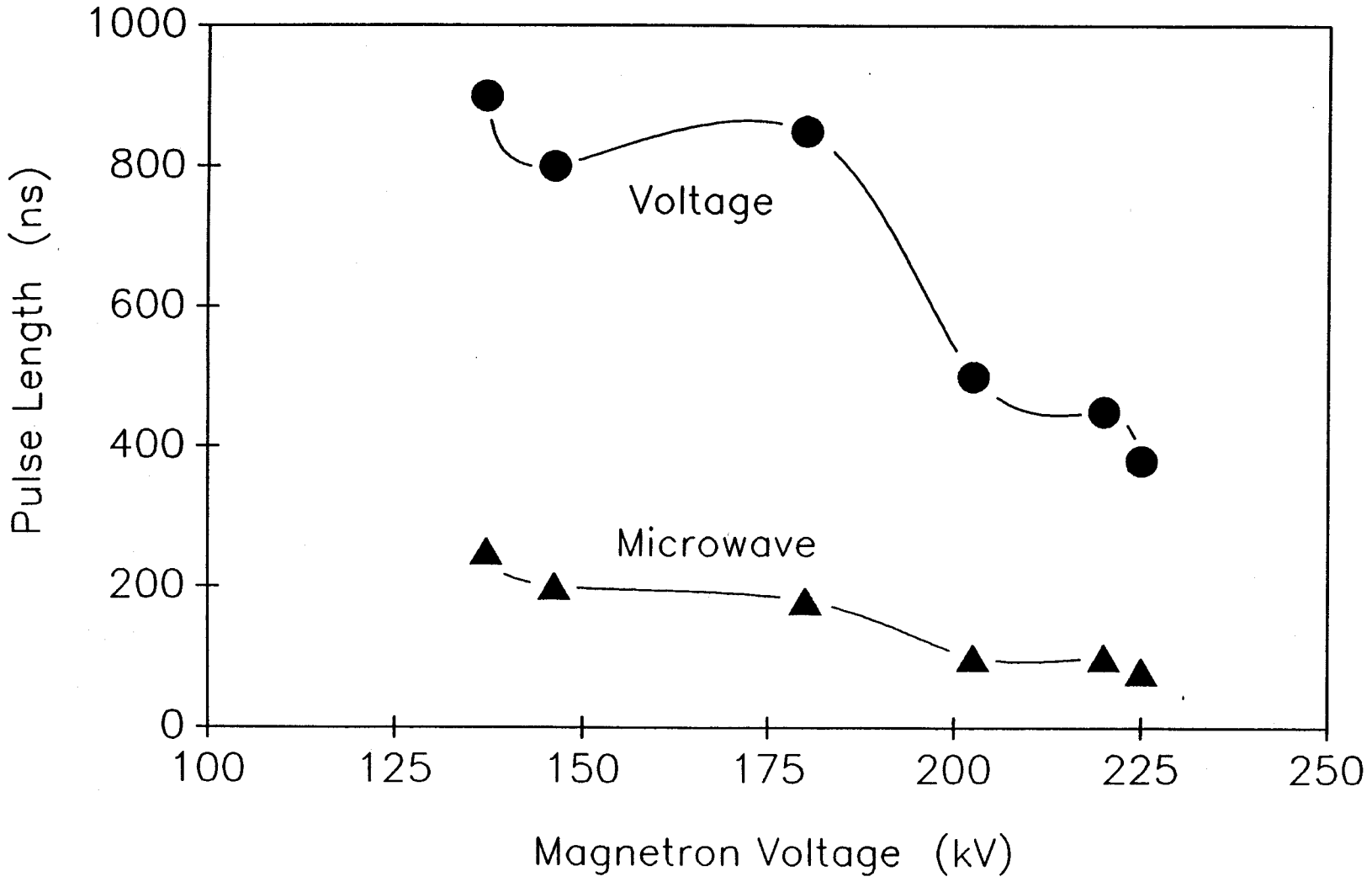
1000
800
600
400
200
0
Pulse Length (ns)
Voltage
Microwave
100
125
150
175
200
225
250
Magnetron Voltage (kV)

Fig. 6

(a)

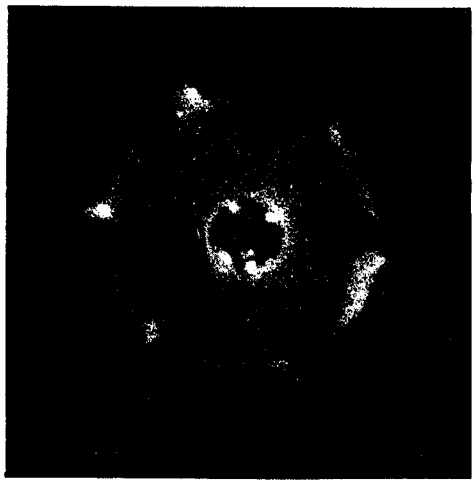

(b)

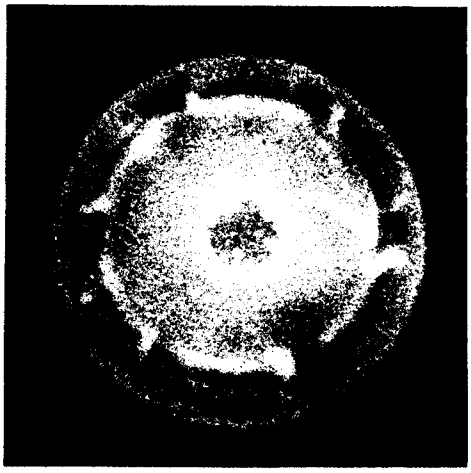

(c)

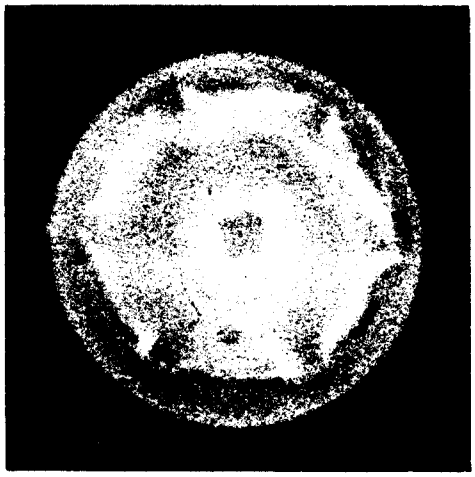

Fig. 7

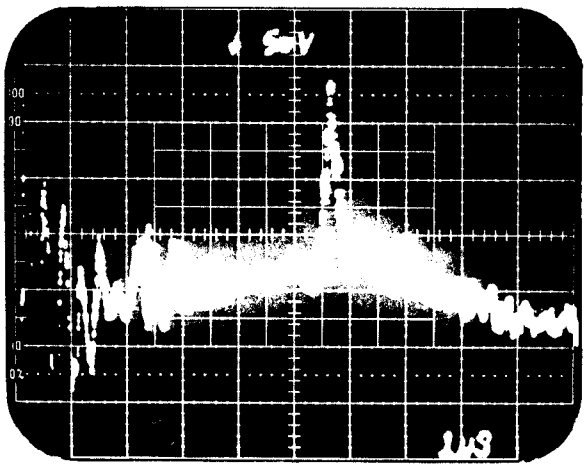

Fig. 8